Journal of Environmental Chemical Engineering 9 (2021) 105096

Contents lists available at ScienceDirect

Journal of Environmental Chemical Engineering

journal homepage: www.elsevier.com/locate/jece

Size effect of hematite particles on the Cr(VI) reduction by *Shewanella oneidensis* MR-1

Abdelkader Mohamed [a,b], Boya Sun [a], Cheng Yu [a], Xuemeng Gu [a], Noha Ashry [a], Yassine Riahi [a], Ke Dai [a,*,1], Qiaoyun Huang [a]

[a] Key Laboratory of Arable Land Conservation (Middle and Lower Reach of Yangtze River), Ministry of Agriculture and Rural Affairs, College of Resources and Environment, Huazhong Agricultural University, Wuhan 430070, PR China
[b] Soil and Water Research Department, Nuclear Research Center, Atomic Energy Authority, Abou Zaabl 13759, Egypt

ARTICLE INFO

Editor: Dr. Zhang Xiwang

Keywords:
Hematite particle size
Shewanella oneidensis MR-1
Cr(VI) reduction
Microcalorimetry
2D-COS studies

ABSTRACT

Microorganisms are commonly bonded to various soil minerals, which may influence the redox processes and bacterial metabolism. However, little is known about the impact of particle size of soil minerals on these redox processes in the subsurface environment. In this study, the Cr(VI) bioreduction by *Shewanella oneidensis* MR-1 (*S. oneidensis*) was investigated in the presence of various hematite (α-Fe_2O_3) particles with average diameters of 1.0 μm (hem-1 μm) and 80.0 nm (hem-80 nm) under different pH conditions. Fourier transformed infrared spectroscopy coupled with two-dimensional correlation spectroscopy (FTIR-2D-COS) analysis and isothermal titration calorimetry (ITC) were used to explore the interaction between *S. oneidensis* and hematite and monitor the bacterial metabolic activity, respectively. X-ray photoelectron spectroscopy (XPS) was used to elucidate the Cr(VI) removal mechanisms. Our results showed that 78% of chromate can be reduced to Cr(III) by *S. oneidensis* alone. Whereas, chromate reduction rates were 62% and 85% in the presence of hem-1 μm and hem-80 nm, respectively. The enhancement of Cr(VI) reduction by *S. oneidensis*-hem-80 nm complex may be due to the large surface area as well as the positive charge of hem-80 nm at neutral pH, which influences the physical contact between *S. oneidensis* and iron oxides. The microcalorimetric results showed that both hem-1 μm and hem-80 nm promoted the normal physiological functions of *S. oneidensis*. XPS confirmed the gradual $FeCr_2O_4$ formation and Fe(II) depletion during the Cr(VI) reduction process. This work expands our understanding of microbial-mineral interaction and its role in Cr(VI) removal mechanisms in the subsurface environment.

1. Introduction

Chromium (Cr), has become a hot area of interest due to its mounting release into the environment from various industrial activities such as wood preservation, leather tanning, electroplating, alloy manufacturing, pigment, and dye synthesis [1]. Chromium mainly exists in two valence states: hexavalent Cr(VI) and trivalent Cr(III) forms in the contaminated environment [2]. Since Cr(VI) is more toxic, soluble, mobile, and carcinogenic than Cr(III), therefore, it is highly recommended to convert Cr(VI) to Cr(III) due to the low toxicity, solubility, and mobility of Cr(III) as well as its precipitation potential as Cr(III) (oxy)hydroxides [3–5].

Microbial Cr(VI) reduction has been regarded as the most suitable chromium remediation approach because of the natural widespread bacteria in the soil and water environment under anaerobic conditions. Moreover, it has been reported that the Cr(VI) bioreduction is a more eco-friendly strategy than the conventional physico-chemical strategies which often result in secondary sludge [6,7]. Recently, many bacteria have been reported to reduce the more toxic Cr(VI) to less toxic Cr(III) including dissimilatory metal reducing bacteria (DMRB) [8,9]. It is well known that the functional groups such as hydroxyl, carboxyl, amino, etc., which are important participants in the biological adsorption process on the surface of microbial cell walls are influenced by the system pH [10].

Iron minerals are ubiquitous in the soil environment and have a high surface area and surface activity, which can be used for heavy metal remediation due to their high redox activity [11,12]. A previous study demonstrated that the effect of minerals on the microbial Cr(VI)

* Corresponding author.
E-mail address: dk@mail.hzau.edu.cn (K. Dai).
[1] ORCID: 0000–0003-0727–0399

https://doi.org/10.1016/j.jece.2021.105096
Received 4 November 2020; Received in revised form 30 December 2020; Accepted 17 January 2021
Available online 18 January 2021

reduction is directly related to the composition and properties of minerals themselves [13]. Hematite minerals play critical roles in mediating electron transfer processes in subsurface environments [14]. It has been reported that the small particle size of hematite has a high density of active sites and a clear antiseptic role [15]. The microbial reduction of Fe(III) oxides is linearly correlated with the surface area and solid-phase surface site concentrations [16]. Further study showed that the minerals particle size can affect the interaction between hematite and c-cell pigments in the main DMRB trans-membrane electron transfer network [17]. In addition, the microbial-iron minerals system has a synergy effect due to the adsorption potential of minerals and microbial reduction capacity. Furthermore, the Fe(II) produced from the microbial reduction of Fe(III) oxides can indirectly reduce Cr(VI) [18]. However, little is known about the size effect of hematite particles on the microbial removal of chromate and bacterial metabolic activity.

In this study, we speculated that iron minerals with different particle size may affect the bacterial activity, the microbial-mineral interaction, and the redox reactions. The main objective is to gain an in-depth understanding of soil mineral-microbes interaction and their effects on bacterial metabolism and chromium reduction. Therefore, in this study, *Shewanella oneidensis* MR-1 was selected as a gram-negative DMRB which can use small amounts of lactate as an electron donor, and various metal ions such as chromium as electron acceptors to achieve the reduction of heavy metals [19]. The effect of hematite particle size on chromium reduction by *S. oneidensis* was investigated. Additionally, bacterial metabolism as influenced by different concentrations of hematite was detected under various pH conditions. Furthermore, the adhesion mechanism of bacterial cells to hematite with different particle sizes was also explored.

2. Materials and methods

2.1. Materials

All chemicals used in this work were analytical grade and all solutions were prepared using deionized water (resistivity 18.2 MΩ·cm). Potassium chromate ($KCrO_4$; Sigma–Aldrich) was used to prepare the Cr (VI) stock solution. All butyl rubber stopper bottles, solutions, and growth media were sterilized prior to use. The reaction system was provided with nitrogen and carbon dioxide (N_2: CO_2 = 4:1) after each sampling to maintain the anoxic conditions. The initial pH 7 was adjusted using NaOH/HCI. All stock solutions were stored at 4 °C before use.

2.2. Microorganism culture

Shewanella oneidensis MR-1 was purchased from China Culture Collection (CCTCC, AB 2013238). The test strain was cultured in Luria-Bertani (LB) medium (yeast extract 5.0 g L^{-1}, tryptone 10 g L^{-1}, NaCl 5.0 g L^{-1}) [20]. Under sterile conditions, the strain was incubated in an orbital incubator at 30 °C with continuous trembling at 150 rpm until reaching to early exponential phase. 1% of the culture solution was inoculated to the same medium and cultured under the same conditions for 14 h to logarithmic long. The resultant cultures were centrifuged at 12,000 g for 5 min and then collected in a 10 mM Bis-Tris propane buffer (BTP, Sigma–Aldrich) solution. The wet bacteria were then mixed in the same buffer, and the resulting bacterium suspension was preserved at 4 °C. The bacterial mass concentration was determined based on the dry weight method.

2.3. Hematite synthesis and characterization

Large-particle hematite (particle size <5 μm, product number 310050) was purchased from Sigma Aldrich. Small-particle hematite (~80 nm) was synthesized using the forced hydrolysis of ferric nitrate. Briefly, 40 g $Fe(NO_3)\cdot 9H_2O$ was dissolved in 500 mL of preheated distilled water to 90 °C. 300 mL of 1.0 M KOH and 50 mL of preheated 1.0 M $NaHCO_3$ solution were directly added into $Fe(NO_3)\cdot 9H_2O$ suspension. The suspension pH was adjusted to 8–8.5 at 90 °C for 48 h. The resulting mineral suspension was cooled overnight, purified by the dialysis 3–4 times per day until its conductivity was reduced to <15 μS/cm. At last, the resulting dense suspension was centrifuged, dried, and ground over 100 sieves.

The hematite samples were characterized using powder X-ray diffraction (XRD), scanning electron microscopy (SEM), and BET surface area measurements according to Burstein G.T., [21]. XRD analysis of hematite samples was performed on an X-ray diffraction meter (D8-ADVANCE of Bruker, Germany) with CuKa target radiation, speed 2 °/min, step length 0.01, voltage 40 kV, and current 40 mA. Hematite samples were analyzed and identified using powder pressure tablet methods. The surface morphology of different particle sizes of hematite was explored using SEM. The samples were centrifuged, washed three times, and then dehydrated step by step with gradient concentrations of ethanol solution (30%, 50%, 70%, 80%, 95%, and 100%) for 15 min at each stage and freeze-dried. A suitable amount of dry powder sample adhered to the scanning electron microscope stage with a conductive adhesive. Surface morphology was observed by a Zeiss EV0 LS10 SEM (Carl Zeiss, Britain). Specific surface area (SSA) of hematite particles were measured based on the N_2 isothermal adsorption method (Quantachrome Autosorb-1, JEDL-6390/LV). Hematite particles of different sizes were suspended in 10 mM BTP buffer (pH 7), and the mineral particles were dispersed in the ultrasonic water bath for 30 min until complete dispersion.

2.4. Preparation of S. oneidensis-hematite complex

Hematite and *S. oneidensis* bacteria were mixed in a certain proportion of mass concentration in a 50 mL butyl rubber stopper bottle and the initial pH was regulated using 1.0 M NaOH/HCl. Nitrogen and carbon dioxide (N_2: CO_2 = 4:1) was injected into the system to provide the anaerobic condition. The composite system was incubated in an orbital incubator at 30 °C and 150 rpm for 2 h to achieve equilibrium in the suspension of the bacteria-mineral complex.

2.5. Determination of surface charge and surface sites

The surface charge of hematite particles and their combination with bacteria was investigated by measuring the zeta potential of the single and binary complexes using zeta potential analyzer (Zetasizer Nano ZEN 3600). At different pH values, 1.0 g L^{-1} of hematite suspension was added to the bacterial cell and the zeta potential was measured. Zeta potential values were recorded three times and the average value was taken.

Potentiometric titration experiments were carried out to detect the surface sites of *S. oneidensis*-hematite complexes. 40 mL of *S. oneidensis*-hematite complexes suspension was added to the potentiometric titration pool and 10 mM HNO_3 was added to titrate the system to pH 4 and stabilize it for 30 min and 10 mM NaOH was used to titrate the system to pH 10. During the passage of high purity N_2, the sample cell was sealed. 1.0 g L^{-1} single mineral suspension was used for the preparation of the complex and 10 mM NaCl was used as the electrolyte background.

2.6. Cr(VI) reduction kinetic experiments

Cr(VI) reduction experiments were carried out in 50 mL butyl rubber stopper bottles containing 1.0 g L^{-1} of *S. oneidensis* (1.918×10^8 cell/mL) and 1.0 g L^{-1} of hematite particles. The effects of hematite particle size and the initial pH on the Cr(VI) reduction were investigated. 5.0 mM Cr(VI) was added as the initial chromium concentration. The initial pH was adjusted to 7 by NaOH/HCI solutions. Nitrogen and carbon dioxide (N_2: CO_2 = 4:1) were inserted to provide the anaerobic condition. A control treatment (without hematite) was set in parallel to explore the

stimulation/inhibition effect of different particle sizes of hematite on Cr (VI) reduction. The effect of initial solution pH on the Cr(VI) reduction was studied before and after the zero points of charge (ZPC) of hematite and *S. oneidensis*-hematite complexes. At certain interval times, 2.0 mL aliquots were withdrawn from the reaction solution, centrifuged at 12,000 g, 4 °C for 5 min to measure the Cr(VI) concentration in the supernatant by a UV–Vis spectrophotometer at 540 nm of absorbance. Three parallel experiments were set up and the results were averaged.

2.7. Fe(II) measurement

Biogenic reduced-Fe(II) produced from hematite was detected using the 1,10-phenanthroline method [22]. Regular aliquots were withdrawn with a sterile syringe and nitrogen was injected after the sampling to exhaust oxygen and ensure the anaerobic environment in the reaction system. Samples were centrifuged at 12,000 g for 5 min and Fe(II) content was measured in the supernatant by phenanthroline spectrophotometry. 5.0 mL of Fe(II)-containing supernatant was added to the colorimetric tube and supplemented to 25 mL with distilled water. A 2.5 mL of ammonium acetate buffer and 1.0 mL of phenanthroline solution were added and the solution was shaken well. After 15 min, the colorimetric measurement was performed at a wavelength of 510 nm. Fe(II) alterations in the suspensions of hematite were detected before and after the reaction. Three parallel experiments were set up and the data results were averaged.

2.8. Two-dimensional correlation spectroscopy analysis

2D correlation spectroscopy is a method for extracting useful information from a collection of spectral data obtained from a sample under the influence of some type of external disturbance such as temperature variations or changes in constituent concentration [23]. Fourier transformation infrared spectroscopy (FTIR) coupled with two-dimensional correlation spectroscopy (2D-COS) analysis was used to characterize the *S. oneidensis*-hematite complexes under the perturbation of initial Cr (VI) concentration (0.5, 1.0, 1.5, 2.0 mM). Samples were centrifuged, lyophilized, and then ground and mixed uniformly with KBr in an agate mortar according to a mass ratio of 1: 100. The mixtures were compressed to 13 mm diameter and placed in the sample room of an infrared spectrometer (Nicolet AVAR 330) to obtain an infrared spectrum. The scanning wave number ranged from 800 to 1800 cm^{-1}, the number of scans was 128, and the resolution was 4 cm^{-1}. The infrared spectrum was analyzed using the infrared software (OPUS 6.5). The two-dimensional infrared correlation analysis method was used to determine the sequence of functional groups after the combination between *S. oneidensis* and hematite. The 2D-COS analysis was performed using 2D shige software (Shige Morita, Japan) to analyze and map synchronous and asynchronous spectra.

2.9. Isothermal titration calorimetry (ITC)

Flow calorimetry is a powerful technique for clarifying the heavy metals binding mechanisms on solid surfaces from the perspective of thermodynamics [24]. To elucidate the effect of hematite in different particle sizes on the metabolism of *S. oneidensis*, a TAM III multichannel thermal activity microcalorimeter (Thermometric AB, Sweden) was used to monitor the bacterial activity through metabolic heat flow analysis. All determinations were performed at 28 °C in 4 mL stainless steel ampoules which were sterilized for 20 min at 121 °C before use. The metabolic power-time curves of *S. oneidensis* were continuously recorded in the absence and presence of hematite. Each ampoules containing 0.1 mL of bacterial culture was added into 1.9 mL LB medium introduced with different concentrations (0.0, 0.5, 1.0, 5.0, and 10.0 g L^{-1}) of pre sterilized-hematite minerals. The power-time curve of bacterial metabolism was analyzed to evaluate the effect of different particle sizes of hematite minerals on microbial metabolism.

2.10. XPS analysis

XPS analyses were employed to determine the chemical states of the surface elements bound to cells using an XSAM800 X-ray photoelectron spectroscopy with Mg Kα as an X-ray source. All spectra were drawn and analyzed using the Avantage software, and carbon C1s (EBE = 284.8 eV) was used as the charge calibration standard.

2.11. Statistical analysis

All experiments were performed in a triplicating system. For one treatment, three different bottles have been set. Three measurements were taken each time, and their means and standard deviations were calculated using the software package (SPSS 7.5). Error bars indicate standard deviation on graphs.

3. Results and discussion

3.1. Characterizations of hematite particles

XRD analysis was performed to identify the present phase in the synthesized mineral. XRD patterns of the iron mineral with different particle sizes confirmed the pure phase of hematite and the characteristic peaks are well-matched with the standard PDF card (79–1741 and 87–1165) without other crystalline phases [25]. XRD patterns of hem-80 nm exhibited peak broadening around 25°, an expected phenomenon, and the change of the full-width at half-maximum (FWHM) revealed the different crystalline sizes [17,26] (Fig. 1a,b). This result is in agreement with the values reported for pure α-Fe_2O_3 hematite nanoparticles [27,28].

SEM images revealed that the two samples of hematite particles had an average diameter of 1.0 μm and 80 nm, respectively. It can be seen that hem-1 μm had a compacted-irregular shape while hem-80 nm had a rhombohedral shape (Fig. 1c,d) which concurs with previous studies [16,29]. The external SSA of hem-1 μm and hem-80 nm as measured by the N_2-BET method were 4.838 and 33.1 m^2/g, respectively [30].

3.2. Surface sites analysis of hematite

The titration curves of a single component of *S. oneidensis*, hem-1 μm, and hem-80 nm are presented in Fig. 2a. The amount of OH^- consumed during the titration at pH ranges from 2.5 to 10.0 represents the bacterial buffering ability derived from the protons released from surface acidic chemical moieties [31]. It can be seen that in the pH range of 5–10, the surface site concentration of *S. oneidensis* is greater than that of hematite particles. This result suggests that the ability of the bacterial alone to react with Cr(VI) is higher than that of hem-1 μm and hem-80 nm.

After the equal-ratios combination of *S. oneidensis* bacteria with hem-1 μm and hem-80 nm, the surface sites of the *S. oneidensis*-hematite complexes increases (Fig. 2b, c). Subsequently, the Cr(VI) adsorption potential on the surface of the composite also increases. Therefore, it is suggested that the hematite minerals increase the sites on the surface of the composite which promotes the Cr(VI) adsorption process. The potential titration results of *S. oneidensis*-hem-1 μm and *S. oneidensis*-hem-80 nm complexes with different proportions of bacteria and minerals are also shown in Fig. 2b, c. The 1:5 bacterial-minerals combination ratio declined the surface sites of the complex, which suggested that the high proportion of minerals in the complex decreases the concentration of surface sites, and therefore reduces the adsorption of Cr(VI).

3.3. Effect of particle size of hematite on the Cr(VI) reduction by *S. oneidensis*

Microbial Cr(VI) reduction by *S. oneidensis* was examined in the presence and absence of hematite at a mass ratio of 1:1 (Fig. 3a).

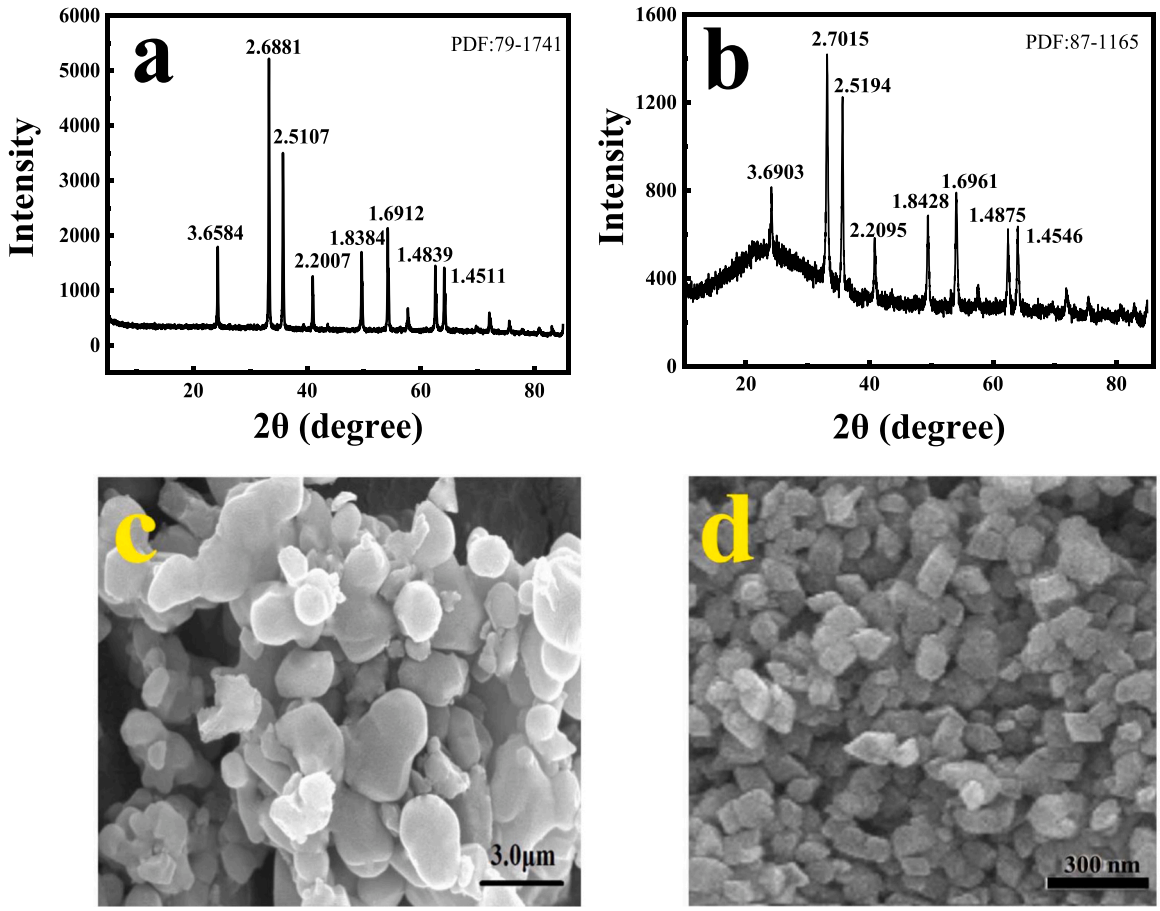

Fig. 1. XRD pattern and SEM images for different hematite particle size samples: hem-1 μm (a, c) and hem-80 nm (b, d) respectively.

S. oneidensis could reduce 83% of chromium after 2 h in the absence of hematite, whereas, Cr(VI) reduction rate was 65% and 91% in the presence of hem-1 μm and hem-80 nm, respectively. This finding suggested that the hem-1 μm significantly inhibited the microbial reduction of Cr(VI), while the hem-80 nm had a moderate promotion effect on the microbial reduction during the first 4 h, revealing that the smaller particle sizes of hematite accelerate the Cr(VI) reduction by *S. oneidensis*-hematite complex. The enhancement of Cr(VI) reduction may be due to the large surface areas as well as the higher reactivity per unit weight, which influences the physical contact between the cells and iron oxides [32]. The hem-1 μm exhibited less cell contact and cell coverage than hem-80 particles, therefore, depressed the electron transfer to Fe(III) oxide particles and thereby declined Cr(VI) reduction rate [16]. Thus, these results confirmed that particle sizes of hematite strongly influenced the microbial reduction of Cr(VI) by *S. oneidensis*. These findings are consistent with a previous study that demonstrated that hematite nanoparticle size can affect Cd(II) sorption on hematite [33]. Bosch et al. [32] confirmed that nano-sized aggregates of iron minerals in colloidal suspensions might be spatially more accessible for microorganisms than large aggregates flocculating as bulk phases.

3.4. Surface charge analysis

Control conditions were set before and after the pH wherein the colloid surface charge is zero which is called the zero point of charge (ZPC), which can explore the promotion or inhibition of the reaction based on the colloid surface charge. By the determination of zeta potential, the ZPC of hem-1 μm and hem-80 nm were 6.0 and 7.3, respectively (Fig. 3b). The colloid surface charge is positive in front of ZPC and negative after ZPC. Therefore, the pH of the reaction system was set to 4, 5, 7, 8, and 6, 7, 8, 9 for the complexes containing hem-1 μm and hem-80 nm, respectively.

The surface charge alterations of the bacterial-minerals complexes before and after the Cr(VI) reduction reaction were also investigated (Table 1). The S. oneidensis-hem-1 μm complex can undergo adsorption and reduction reactions within the chromium removal process. After the reduction reaction, Cr(VI) was converted to Cr(III), which is a positive charge ion and is prone to adsorb to the negative complex surface based on the electrostatic analysis, therefore, the surface positive charge increased after the reaction and negative charge decreased [34].

On the other hand, the surface negative charge of the *S. oneidensis*-hem-80 nm complex increased after the reaction which may be due to the more CrO_4^{2-} adsorption on the positively charged surface of hem-80 nm at pH 7.0 before the reduction process (Fig. 3b). Therefore, the adsorption process may coexist in the reaction system and the surface charge of the complex after the reaction is less than before.

3.5. Biogenic-Fe(II) produced from hematite reduction

The change of biogenic produced-Fe(II) can interpret its crucial role in the Cr(VI) reduction process. The alteration of Fe(II) concentration in the suspension of *S. oneidensis*-hem-1 μm and *S. oneidensis*-hem-80 nm complexes with/without reacting with Cr(VI) was measured (Fig. 3c). It can be seen that in the absence of Cr(VI), *S. oneidensis* can reduce hem-1 μm and hem-80 to produce 1.6 and 7.3 mg L^{-1} Fe(II) after 4 h, respectively. However, in the presence of Cr(VI), the concentration of Fe (II) did not change and remained close to zero throughout the reduction process, possibly due to the following reasons: (1) Fe precipitation during the reduction of Cr(VI), so Fe(II) cannot be detected in the solution; (2) when both Fe(III) and Cr(VI) are present in the reaction

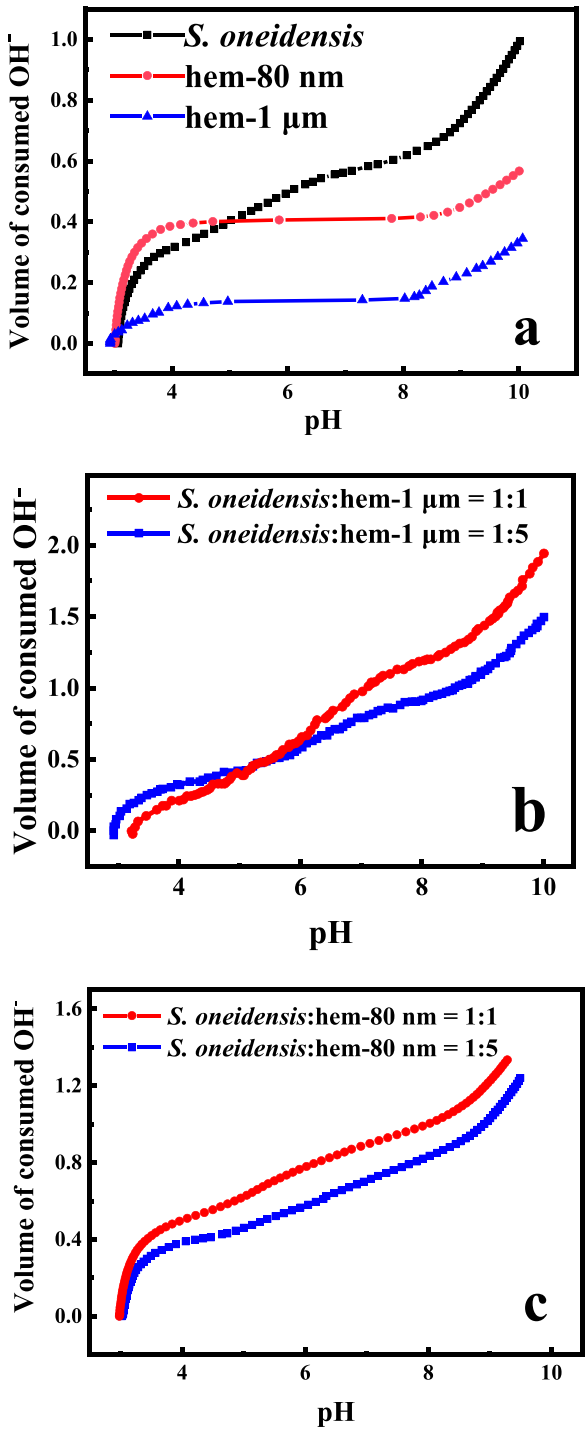

Fig. 2. Potentiometric titration curves of single *S. oneidensis,* hem-1 μm, and hem-80 nm (a); potentiometric titration curves of *S. oneidensis*-hem-1 μm complex (b), and *S. oneidensis*-hem-80 nm complex (c) with different proportions.

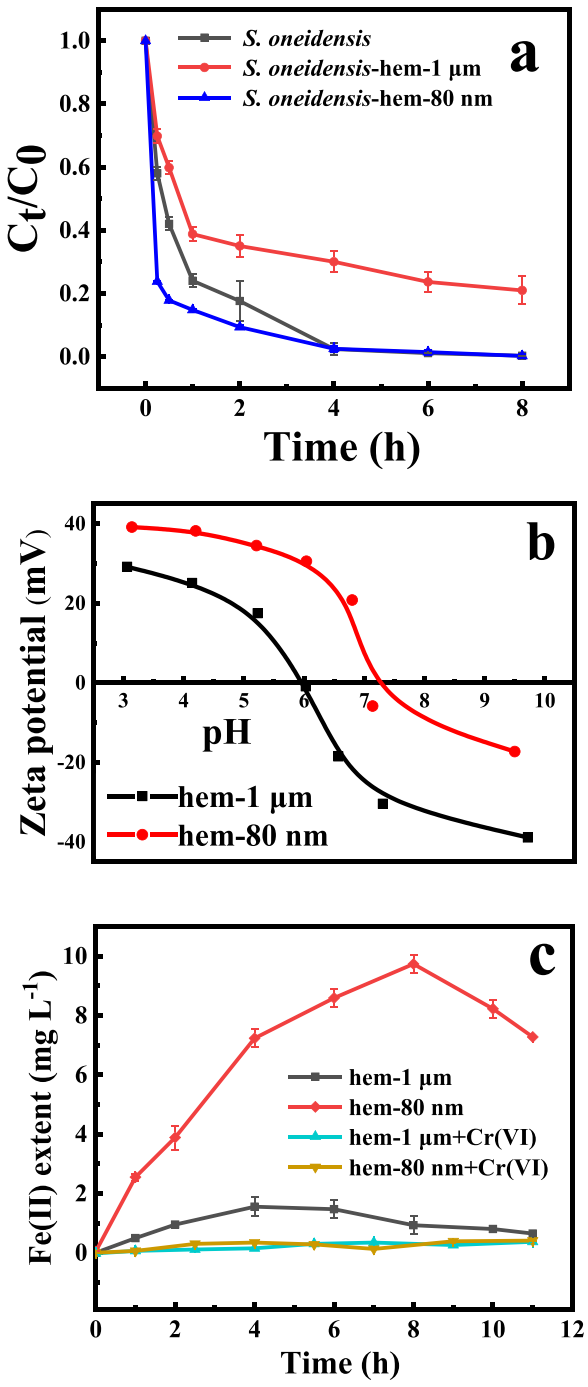

Fig. 3. Effect of hematite particle size on Cr(VI) reduction by *S. oneidensis* and *S. oneidensis*-hematite complexes (a); determination the zero point of charge (ZPC) for different particle sizes of hematite (b); Fe(II) extent vacillation in hem-1 μm and hem-80 nm before/after reacting with Cr(VI) (c).

system, Cr(VI) is preferentially reduced because of the high redox potential of Cr(VI), therefore Cr(VI) acted as the first terminal destination to accept the electrons transferred from bacterial cells; (3) hematite has already been reduced but the biogenic produced-Fe(II) was exhausted in Cr(VI) reduction by an instantaneous abiotic process; (4) the electron donor in the solution is consumed during the reduction of Cr(VI) and is not sufficient to reduce Fe(III) in hematite. However, the kinetic results indicated that the reduction of Cr(VI) by *S. oneidensis* bacteria reached equilibrium in 2–4 h, and the reduction rate could reach 99% proving

Table 1
Surface charge of *S. oneidensis*-hematite composites before and after reaction with Cr(VI).

Complex	Zeta potential (pH 7.0)	
	Before the reaction	After the reaction
S. oneidensis-hem-1 μm	−9.72	−4.49
S. oneidensis-hem-80 nm	−5.38	−12.73

that the amount of electron donors in the reduction system is sufficient and Fe participates during the reduction of Cr(VI), therefore, Fe(II) could not be detected in the presence of Cr(VI) [35].

3.6. Effect of initial pH on the Cr(VI) reduction

Since the initial pH directly influences the surface charge of hematite, the aggregation, and physiological functions of bacteria, the effect of initial pH on the Cr(VI) reduction by pure hematite with different particle sizes and their composites with *S. oneidensis* was investigated. The Cr(VI) removal rate by hem-80 nm is slightly stronger than that of hem-1 μm. However, under different pH, the chromium removal rate by both hematite particles fluctuated within 10–20% and there was no continuous mounting removal of Cr(VI) (Fig. 4a, b). These results revealed that hematite alone did not have a strong affinity to Cr(VI) and surface adsorption was the main mechanism for Cr(VI) removal. As the ZPC of hem-1 μm and hem-80 nm is 6.0 and 7.3, respectively. The hem-1 μm and hem-80 nm are positively charged under acidic conditions which interpreted the surface adsorption process. After the combination of hematite and *S. oneidensis*, the cell surface morphology changed, and the Cr(VI) reduction process was strongly stimulated in comparison with hematite alone (Fig. 4c, d). The reduction extent after the combination is stronger than that of a single hem-1 μm, although the reduction rate is limited. After 1 h of reaction, the reduction equilibrium is primarily reached with about 12.5% of Cr(VI) removed. It is noteworthy that the Cr(VI) reduction efficiency after recombination was significantly improved when the pH value was higher than ZPC. There was about 56% of Cr(VI) reduced in the first hour, and the reduction is still taking place within 10 h. Under this situation, the adsorption was very weak, accounting for less than 1% of Cr(VI) removal. The Cr(VI) reduction by hem-80 nm and *S. oneidensis*-hem-80 nm complex was investigated at different pH (Fig. 4b, d). The Cr(VI) reduction by the nanoparticle of

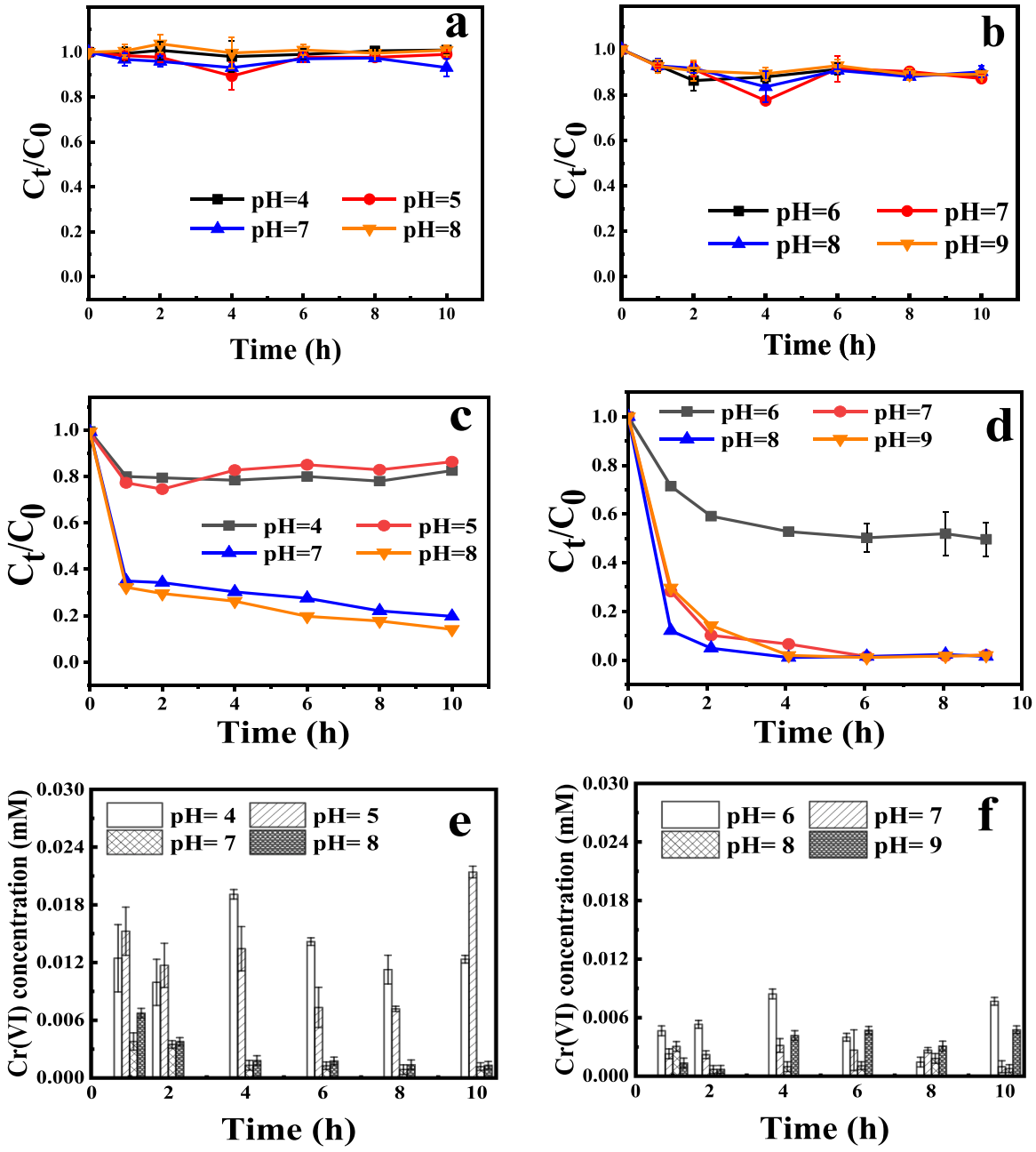

Fig. 4. Effect of initial pH on Cr(VI) reduction by hem-1 μm (a); hem-80 nm (b); *S. oneidensis*- hem-1 μm (c); and *S. oneidensis*-hem-80 nm (d); effect of initial pH on Cr(VI) adsorption by *S. oneidensis*-hem-1 μm and *S. oneidensis*-hem-80 nm complexes (e, f) after 8 h of the reaction process.

hematite is quite stronger than microparticles, and the effect of pH is similar to that of large particle size. After combination with *S. oneidensis*, the reduction rate and conversion rate increased significantly (Fig. 4d). The Cr(VI) removal at pH > ZPC was due to the electrostatic adsorption because of the positive surface charge of the hematite particles which adsorb 10–20% of the negative charged Cr(VI) (Fig. 4a, b). However, after ZPC, the adsorption process did not play a major role owing to the negative charge of hematite particles which lead to surface repulsion with negative charged Cr(VI). The effect of initial pH on the adsorption of Cr(VI) by *S. oneidensis*-hem-1 μm and *S. oneidensis*-hem-80 nm complexes were explored (Fig. 4e, f). It can be seen that the adsorption rates are very low. Moreover, the adsorption rate on the *S. oneidensis*-hem-1 μm complex is stronger than the *S. oneidensis*-hem-80 nm complex, and the adsorption rate is higher before ZPC.

In both complexes, the adsorption process existed but the adsorption time was different. For *S. oneidensis*-hem-1 μm complex, the adsorption process occurred after the microbial reduction of chromate which produces positively charged Cr(III). However, in the reaction system of *S. oneidensis*-hem-80 nm complex, the adsorption potential that occurred before the microbial Cr(VI) reduction is more than after the reduction process may be due to the positive charge of hem-80 nm at neutral pH.

Overall, the combination of *S. oneidensis* and hem-80 nm can promote and accelerate the reduction process, especially after ZPC (pH ≥ 7.0). In neutral and alkali conditions, *S. oneidensis* could reduce 75% and 99% of Cr(VI) within 8 h in the presence of hem-1 μm and hem-80 nm respectively (Fig. 4c, d). It is worth noted that microbial Cr(VI) reduction by *S. oneidensis* was promoted with the increase of pH, possibly as *S. oneidensis* was originally isolated from the alkaline Lake Oneida (pH ≥ 9.1) [36]. pH affects the electrostatic interactions between *S. oneidensis* and hematite where *S. oneidensis* was negatively charged due to its functional groups. The electrostatic attractions between hematite and *S. oneidensis* cells at lower pH are expected to be decreased at higher pH levels. Therefore, the change in pH greatly influences the strength of electrostatic interaction, H-binding, and the amount of attached cells. Subsequently, the Cr(VI) removal is a pH-dependent process due to pH impacts on the cell structure and bacterial-mineral interaction [37].

3.7. Metabolic activity of S. oneidensis in the complexes

A multichannel thermal activity microcalorimeter can monitor bacterial metabolic activity and detect the thermal power of bacterial metabolism. The difference between the heat released by catabolism and the heat absorbed by anabolic metabolism during bacterial metabolism is expressed as bacterial metabolic heat [38]. Two parameters, peak time (PT) and peak height (pH are often used to represent the profiles of the power-time curves. The measured microbial metabolic heat flux showed that the greatest metabolic activity of *S. oneidensis* occurred in the presence of 1.0 g L^{-1} of hematite, regardless of its particle size (Fig. 5a, b). Except for 1.0 g L^{-1}, the presence of different concentrations of hem-1 μm did not change the PT and pH of *S. oneidensis* (Fig. 5a), indicating that the mineral did not have an obvious inhibition effect on the metabolic rate of *S. oneidensis*. Meanwhile, the presence of 1.0 and 10 g L^{-1} of hem-80 nm promoted and prolonged the metabolic activity of *S. oneidensis* (Fig. 5b). Therefore, it is concluded that hematite mineral stimulated the metabolic exothermic of *S. oneidensis*, and hematite has the greatest effect at a concentration of 1.0 g L^{-1}, but does not change the activity of *S. oneidensis* and does not affect the metabolic process. Similar results of the hematite effect on *Bacillus subtilis* BSn5 activity were reported by Ma et al. [39]. The promotion effect of the hematite nanoparticles on microbial activity may be due to the high specific surface areas and large surface reactivity. Additionally, the accumulation of nutrients on the surface of mineral particles and the large buffering capacities which maintained the convenient pH are both beneficial for bacterial growth [40]. Furthermore, in the presence of poorly accessible electron acceptors such as iron oxides, microbes still use those electron acceptors to support their metabolism and growth [41].

3.8. Analysis of functional groups

FT-IR spectra of *S. oneidensis*, *S. oneidensis*-hem-1 μm, and *S. oneidensis*-hem-80 nm complexes were shown in Fig. S1. It can be noticed that the combination of *S. oneidensis* with different hematite particle size did not change the main functional groups on *S. oneidensis* or result in the emergence of new feature peaks. This result suggests that the functional group on *S. oneidensis* is the main functional group in the Cr(VI) removal process [35]. The tendency of peak intensity decrease speculated that Cr(VI) mainly reacted with *S. oneidensis* on the complexes, revealing the vital role of certain functional groups on *S. oneidensis* such as carboxyl and amide groups in the metal-binding process [42].

Two-dimensional correlation spectroscopy is a new type of spectral analysis method, which is based on time-resolved detection of spectral signals and characterizes the mutual relationship of each signal in the process of external perturbation. The relative order of the response of functional groups to the external perturbation conditions can be judged based on the intensity changes of the relevant peaks, and the sequence of the functional groups during the reaction [37]. The red area in the two-dimensional infrared spectrum represents a positive correlation, and the blue area represents a negative correlation. The wavenumber range of 800 cm^{-1}-1800 cm^{-1} was selected, and the combined color distribution of the corresponding area in the map was analyzed to get the correlation order of the response of the functional group. The response order of different functional groups was expressed by the precedence sign (>). The two-dimensional map of the Cr(VI) reduction

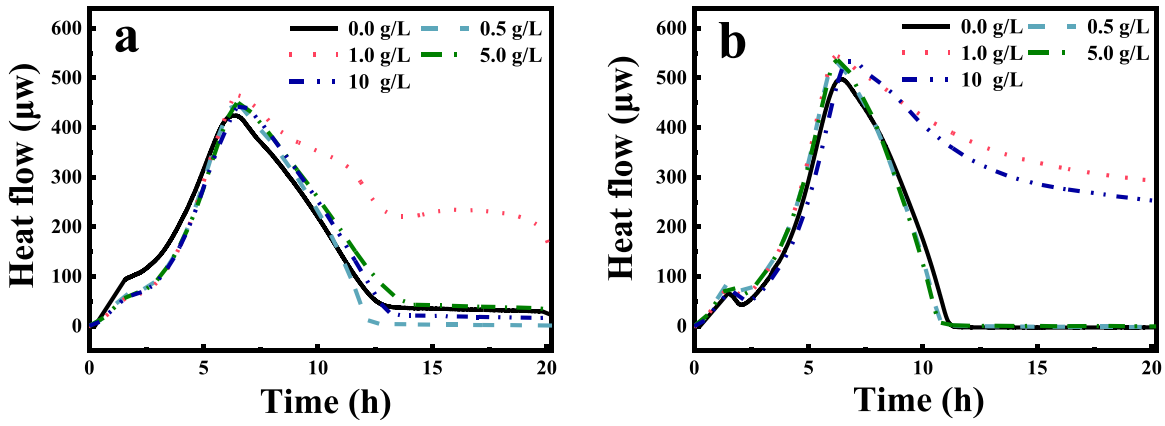

Fig. 5. Power–time curves of *Shewanella oneidensis* MR-1 in the presence of different concentrations of hem-1 μm (a) and hem-80 nm (b).

by the combination of *S. oneidensis* and hem-1 μm with initial Cr(VI) perturbation was shown in Fig. 6a, and b. The correlated bands in the main diagonal are 1640, 1540, 1390, and 1080 cm^{-1} band. According to the Noda rule, the correlation priority of the four bands is: 1080 > 1640 > 1540 > 1390 cm^{-1}, indicating the sequence of the corresponding functional groups reacted with Cr(VI) is monodentate complex PO_2 >amide I >amide II >COO^-. The two-dimensional spectrum of Cr(VI) reduction by the *S. oneidensis*-hem-80 nm complex was detected and displayed in Fig. 6c, and d. It can be seen that there are obvious correlations in the four bands of 1640, 1540, 1080, 1240 cm^{-1}. The priority order is: 1640 > 1540 > 1080 > 1240 cm^{-1}. The corresponding functional groups are amide I >amide II >monodentate complex PO_2 > MR-1 PO_2. This reaction sequence demonstrated that the order in which the bacterial functional groups interact with hematite is closely related to the particle size [43].

3.9. Characterization of Cr(VI) removal mechanisms using XPS

XPS is used to investigate the elemental composition and chemical states of surface and near-surface species. XPS spectra of *S. oneidensis*-hem-80 nm complex before and after reacting with 1.0 mM Cr(VI) are shown in Fig. 7. The total survey spectrum of the pristine complex indicated that the main elements at the complex surface are carbon (65.46%), oxygen (30.78%), and iron (3.77%) (Fig. 7a). After reacting with Cr(VI) for 10 h, new peaks appeared around 580 eV, which are assigned to the photoelectron peaks of chromium and elucidate the absorption of chromium on the complex surface [44]. Fe content decreased from 3.77% to 2.34% after reacting with Cr(VI) for 10 h, confirming the vital role of generated Fe(II) in the chromium reduction process which is consistent with the reduction kinetic results (Fig. 3a, c). These results interpret why Cr(VI) removal efficiencies by *S. oneidensis* and *S. oneidensis*-hem-80 nm complex were 80% and 90%, respectively. These phenomena revealed that the *S. oneidensis*-hem-80 nm complex stimulate Cr(VI) bio removal by 10% due to generated Fe(II) [45]. The carbon peaks of the complex were likely attributed to hydrocarbon and/or CO_2 contamination during sample preparation [46]. Fig. 7b showed that the C 1s spectrum exhibited photoelectron peaks at 284.7, 286.01, and 288.16 eV which attributed to C–H or C–C, C–O–C, and O–C=O, respectively [35,47]. In the C 1s spectrum of *S. oneidensis*-hem-80 nm complex before and after the reaction, the peak area of O–C=O and O–C=O decreased from 32.47% and 14.50–26.64% and 12.03%, respectively. Nevertheless, the peak area of C–C increased from 53.03% to 61.33%. These slight changes in peak areas were due to the Cr(VI) reduction by the organic carbon groups [48]. The Fe 2p spectrum of the *S. oneidensis*-hem-80 nm complex (Fig. 7c) clearly authenticate the existence of both Fe(II) at 710.3 eV attributed to Fe^{2+}octa (31.94%) and Fe(III) at both 711.8 and 723.93 eV represented by Fe^{3+} octa (35.29%) and Fe_2O_3 (24.85%), respectively [45,49]. After 10 h reaction, a peak at 710.6 eV was emerged, which are ascribed to the Fe 2p of $FeCr_2O_4$ [50], proving the formation of $FeCr_2O_4$. The intensities of the two peaks at 711.8 and 723.93 eV increased from 35.29% and 24.85–44.08% and 28.39%, respectively. However, 31.94% of Fe^{2+}octa peak intensity was completely consumed and disappeared after a 10 h reaction. These results emphasized that the amount of $FeCr_2O_4$

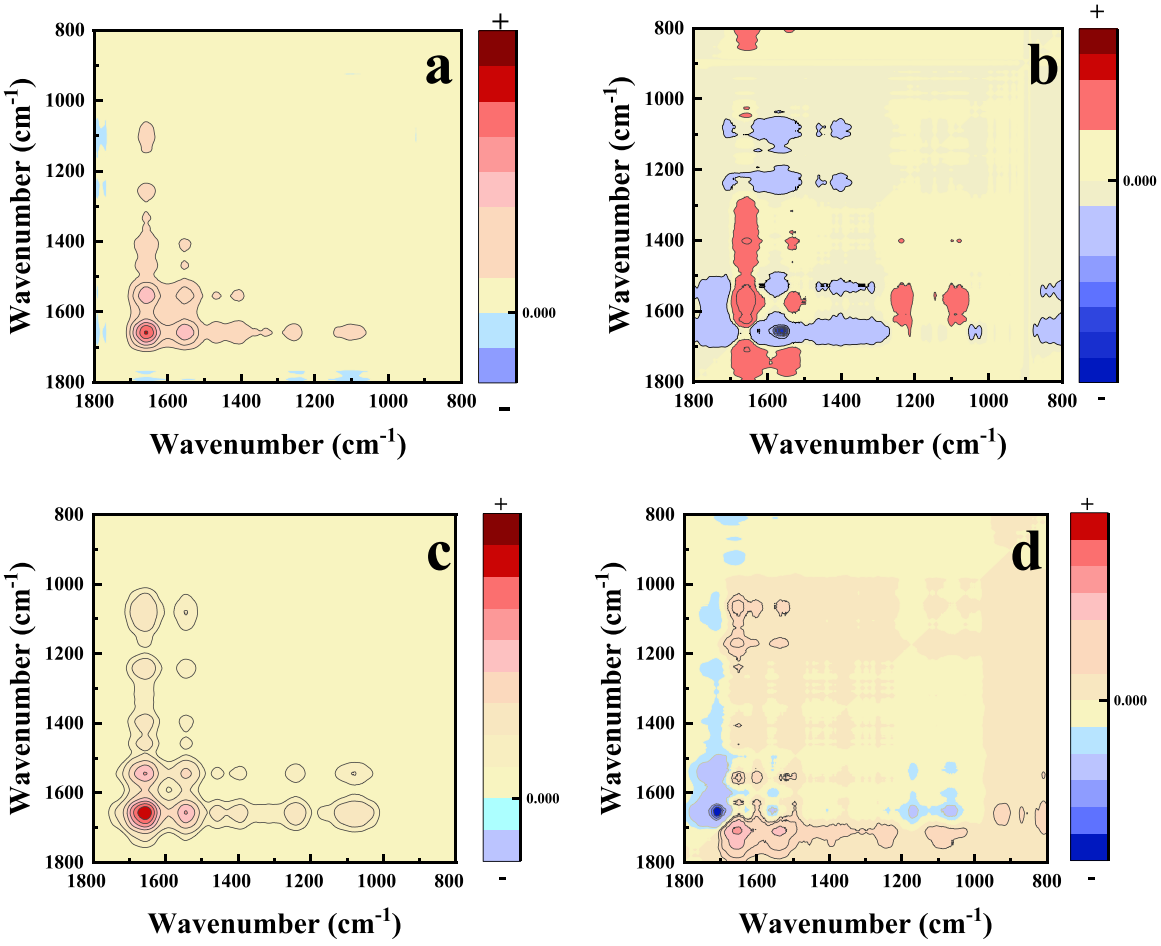

Fig. 6. Synchronous (left) and asynchronous (right) 2D correlation contour maps of *S. oneidensis*-hem-1 μm complex (a, b) and *S. oneidensis*-hem-80 nm complex (c, d) after Cr(VI) reduction with the perturbation of Cr(VI) concentration. The red and blue regions represent positive and negative correlations, respectively. (For interpretation of the references to colour in this figure legend, the reader is referred to the web version of this article.).

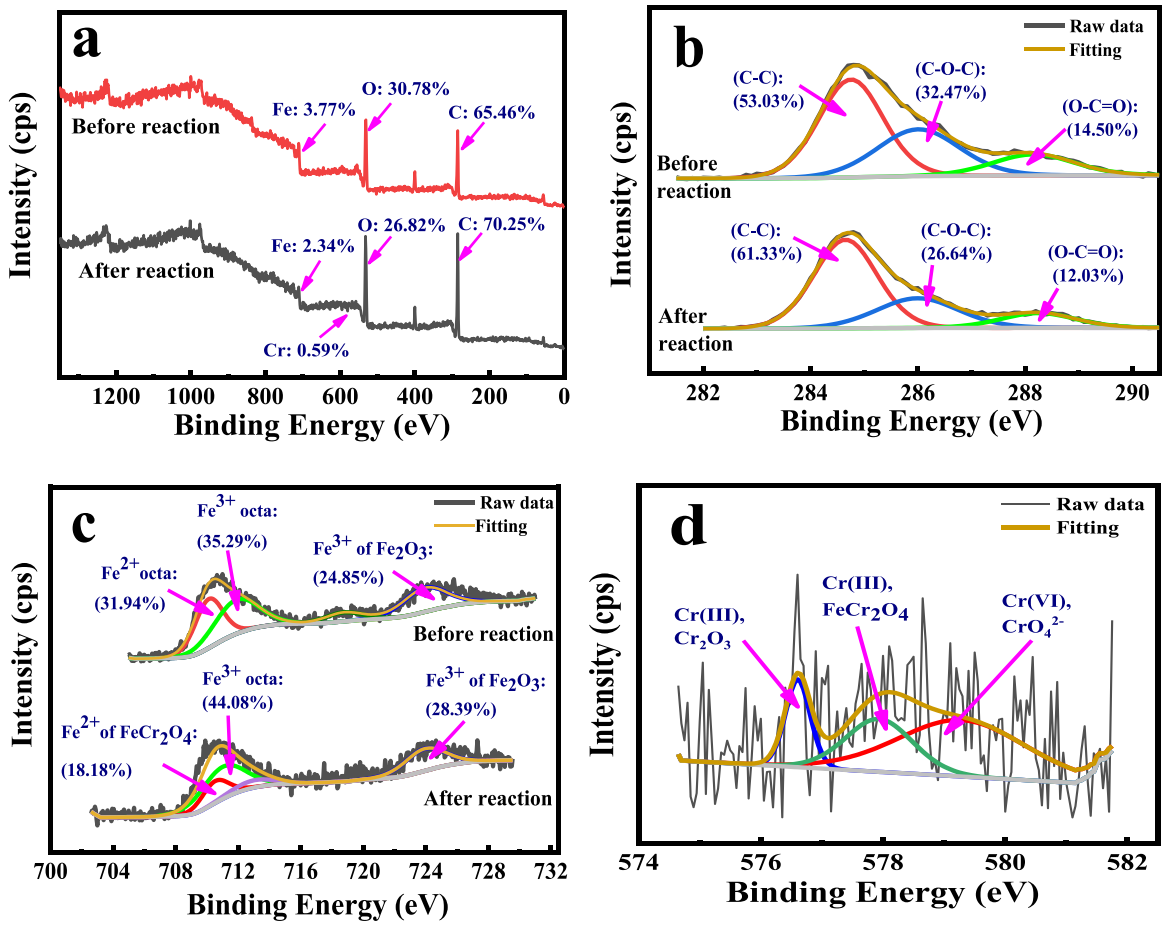

Fig. 7. High-resolution XPS analyses of total survey scan (a); C 1 s (b); Fe 2p (c); and Cr 2p (d) of *S. oneidensis*-hem-80 nm before/after 10 h of reaction with 1.0 mM of Cr(VI) under anoxic condition. C 1 s photopeak at 284.8 eV was used as a reference for all spectra.

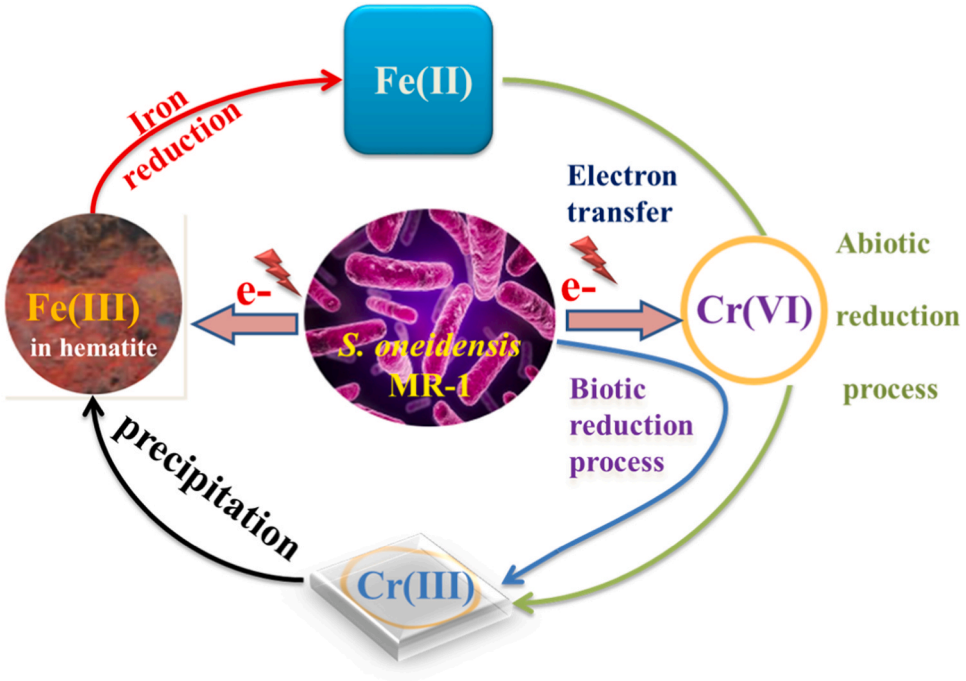

Fig. 8. Schematic diagram for Cr(VI) reduction mechanisms by *S. oneidensis* in the presence of hematite minerals.

was progressively produced, whereas the amount of Fe(II) was gradually depleted during the Cr(VI) reduction process by *S. oneidensis*-hem-80 nm complex [45]. As shown in Fig. 7d, the Cr 2p spectrum of *S. oneidensis*-hem-80 nm complex obviously illustrated that the Cr 2p peaks at 576.61, 577.94, and 579.29 eV correspond to Cr_2O_3, $FeCr_2O_4$, and Cr(VI) of CrO_4^{2-}, respectively. It suggests the simultaneous adsorption and reduction during the Cr(VI) removal [51]. The presence of both Cr(III) and Cr(VI) on the surface of *S. oneidensis*-hem-80 nm complex confirmed that both adsorption and reduction contributed to the Cr(VI) removal from aqueous solution, but the redox reaction was the dominant reason for Cr(VI) removal. Therefore, based on the above results, the proposed mechanism of the Cr(VI) removal by the *S. oneidensis* in the presence of hematite mineral under anoxic condition generally includes three steps (i) adsorption, (ii) reduction, and (iii) co-precipitation [52] as shown in Fig. 8. First, Cr(VI) oxyanions are rapidly adsorbed to the surface of the hem-80 nm because of the large surface area and positively charged surface at a neutral pH level. Second, direct biotic reduction by *S. oneidensis* and indirect abiotic reduction of Cr(VI) by the bio-produced Fe(II), which extend the electrons transfer to reduce Cr(VI) to Cr(III) simultaneously. Finally, the produced Cr(III) oxyanions co-precipitated on the complex surface which demonstrated the merit of chromate non-oxidizing potential.

4. Conclusions

This study investigated the effect of hematite particle size on Cr(VI) reduction by *Shewanella oneidensis* MR-1 under different pH conditions. The *S. oneidensis*-hem-80 nm complex accelerates the Cr(VI) reduction process, whereas the *S. oneidensis*-hem-1 μm complex inhibited the Cr (VI) reduction process due to the smaller specific surface area and the weaker adsorption capacity of hem-1 μm. Cr(VI) removal is a pH-dependant process as pH significantly influences the electrostatic interactions between *S. oneidensis* cells and hematite particles. Hematite can promote the exothermic of *S. oneidensis* metabolism and has the greatest effect at a concentration of 1.0 g L^{-1} of both particle sizes but does not change the microbial activity of *S. oneidensis*. The functional groups on the surface of *S. oneidensis* are the main functional group in the Cr(VI) removal process revealing the vital role of certain functional groups of *S. oneidensis* such as carboxyl and amide groups in the metal-binding process. Therefore, this study demonstrated that the particle size of hematite affected the microbial reduction of chromate and microbial activity under various pH levels. Furthermore, simultaneous biotic and abiotic reduction of Cr(VI) occurs by bacteria and bio-produced Fe(II), respectively. Cr(III) oxyanions were produced and co-precipitated to the complex surface. Thus, this study provides a clear insight into the Cr(VI) removal kinetics and mechanisms and affords a possible method for the Cr(VI) remediation.

Funding

The research was financially supported by the National Natural Science Foundation of China (41671230, 42077017).

CRediT authorship contribution statement

Abdelkader Mohamed: Performing experiments, Data curation, Writing - original draft. **Ke Dai:** Conceptualization, Methodology. **Boya Sun:** Performing experiments, Investigation. **Xuemeng Gu:** Performing experiments, Investigation. **Cheng Yu**: Performing experiments, Investigation. **Noha Ashry:** Visualization, Investigation, Software, Validation. **Yassine Riahi**: Visualization, Investigation, Software, Validation. **Qiaoyun Huang:** Writing - review & editing. The manuscript was written through contributions of all authors, each of whom has approved the final version of the manuscript.

Declaration of Competing Interest

The authors declare that they have no known competing for financial interests or personal relationships that could have appeared to influence the work reported in this paper.

Acknowledgments

The authors would like to thank and appreciate the financial support of the National Natural Science Foundation of China (41671230, 42077017).

Appendix A. Supporting information

Supplementary data associated with this article can be found in the online version at doi:10.1016/j.jece.2021.105096.

References

[1] J. Qian, J. Zhou, L. Wang, L. Wei, Q. Li, D. Wang, Q. Wang, Direct Cr (VI) bio-reduction with organics as electron donor by anaerobic sludge, Chem. Eng. J. 309 (2017) 330–338, https://doi.org/10.1016/j.cej.2016.10.077.
[2] R. Bencheikh-Latmani, A. Obraztsova, M.R. Mackey, M.H. Ellisman, B.M. Tebo, Toxicity of Cr(III) to *Shewanella* sp. strain MR-4 during Cr(VI) reduction, Environ. Sci. Technol. 41 (2007) 214–220, https://doi.org/10.1021/es0622655.
[3] N. Habibul, Y. Hu, Y.K. Wang, W. Chen, H.Q. Yu, G.P. Sheng, Bioelectrochemical chromium(VI) removal in plant-microbial fuel cells, Environ. Sci. Technol. 50 (2016) 3882–3889, https://doi.org/10.1021/acs.est.5b06376.
[4] S. Li, L. Tang, G. Zeng, J. Wang, Y. Deng, J. Wang, Z. Xie, Y. Zhou, Catalytic reduction of hexavalent chromium by a novel nitrogen-functionalized magnetic ordered mesoporous carbon doped with Pd nanoparticles, Environ. Sci. Pollut. Res. 23 (2016) 22027–22036, https://doi.org/10.1007/s11356-016-7439-x.
[5] W. Wang, B. Zhang, Q. Liu, P. Du, W. Liu, Z. He, Biosynthesis of palladium nanoparticles using: *Shewanella loihica* PV-4 for excellent catalytic reduction of chromium(VI), Environ. Sci. Nano 5 (2018) 730–739, https://doi.org/10.1039/c7en01167a.
[6] U. Thacker, D. Madamwar, Reduction of toxic chromium and partial localization of chromium reductase activity in bacterial isolate DM1, World J. Microbiol. Biotechnol. 21 (2005) 891–899, https://doi.org/10.1007/s11274-004-6557-7.
[7] C.E. Barrera-Díaz, V. Lugo-Lugo, B. Bilyeu, A review of chemical, electrochemical and biological methods for aqueous Cr(VI) reduction, J. Hazard. Mater. 223–224 (2012) 1–12, https://doi.org/10.1016/j.jhazmat.2012.04.054.
[8] Y. Tuo, G. Liu, J. Zhou, A. Wang, J. Wang, R. Jin, H. Lv, Microbial formation of palladium nanoparticles by *Geobacter sulfurreducens* for chromate reduction, Bioresour. Technol. 133 (2013) 606–611, https://doi.org/10.1016/j.biortech.2013.02.016.
[9] D. Pradhan, L.B. Sukla, M. Sawyer, P.K.S.M. Rahman, Recent bioreduction of hexavalent chromium in wastewater treatment: a review, J. Ind. Eng. Chem. 55 (2017) 1–20, https://doi.org/10.1016/j.jiec.2017.06.040.
[10] S. Chhikara, A. Hooda, L. Rana, R. Dhankhar, Chromium (VI) biosorption by immobilized *Aspergillus niger* in continuous flow system with special reference to FTIR analysis, J. Environ. Biol. 31 (2010) 561–566.
[11] M.F. Horst, V. Lassalle, M.L. Ferreira, Nanosized magnetite in low cost materials for remediation of water polluted with toxic metals, azo- and antraquinonic dyes, Front. Environ. Sci. Eng. 9 (2015) 746–769, https://doi.org/10.1007/s11783-015-0814-x.
[12] Y. Gong, J. Tang, D. Zhao, Application of iron sulfide particles for groundwater and soil remediation: a review, Water Res. 89 (2016) 309–320, https://doi.org/10.1016/j.watres.2015.11.063.
[13] E.E. Roden, Fe(III) oxide reactivity toward biological versus chemical reduction, Environ. Sci. Technol. 37 (2003) 1319–1324, https://doi.org/10.1021/es026038o.
[14] T. Liu, Y. Wang, C. Liu, X. Li, K. Cheng, Y. Wu, L. Fang, F. Li, C. Liu, Conduction band of hematite can mediate cytochrome reduction by Fe(II) under dark and anoxic conditions, Environ. Sci. Technol. 54 (2020) 4810–4819, https://doi.org/10.1021/acs.est.9b06141.
[15] Y.T. He, J. Wan, T. Tokunaga, Kinetic stability of hematite nanoparticles: the effect of particle sizes, J. Nanopart. Res. 10 (2008) 321–332, https://doi.org/10.1007/s11051-007-9255-1.
[16] S. Bose, M.F. Hochella, Y.A. Gorby, D.W. Kennedy, D.E. McCready, A.S. Madden, B. H. Lower, Bioreduction of hematite nanoparticles by the dissimilatory iron reducing bacterium *Shewanella oneidensis* MR-1, Geochim. Et. Cosmochim. Acta 73 (2009) 962–976, https://doi.org/10.1016/j.gca.2008.11.031.
[17] J. Liu, C.I. Pearce, L. Shi, Z. Wang, Z. Shi, E. Arenholz, K.M. Rosso, Particle size effect and the mechanism of hematite reduction by the outer membrane cytochrome OmcA of *Shewanella oneidensis* MR-1, Geochim. Et. Cosmochim. Acta 193 (2016) 160–175, https://doi.org/10.1016/j.gca.2016.08.022.
[18] Y. Wang, P.C. Sevinc, S.M. Belchik, J. Fredrickson, L. Shi, H.P. Lu, Single-cell imaging and spectroscopic analyses of Cr(VI) reduction on the surface of bacterial cells, Langmuir 29 (2013) 950–956, https://doi.org/10.1021/la303779y.

[19] S.S. Middleton, R.B. Latmani, M.R. Mackey, M.H. Ellisman, B.M. Tebo, C.S. Criddle, Cometabolism of Cr(VI) by *Shewanella oneidensis* MR-1 produces cell-associated reduced chromium and inhibits growth, Biotechnol. Bioeng. 83 (2003) 627–637, https://doi.org/10.1002/bit.10725.
[20] C. Li, X. Yi, Z. Dang, H. Yu, T. Zeng, C. Wei, C. Feng, Fate of Fe and Cd upon microbial reduction of Cd-loaded polyferric flocs by *Shewanella oneidensis* MR-1, Chemosphere 144 (2016) 2065–2072, https://doi.org/10.1016/j.chemosphere.2015.10.095.
[21] G.T. Burstein, Iron oxides in the laboratory, Prep. Charact. (1992), https://doi.org/10.1016/0010-938x(92)90174-2.
[22] H. Tamura, K. Goto, T. Yotsuyanagi, M. Nagayama, Spectrophotometric determination of iron(II) with 1,10-phenanthroline in the presence of large amounts of iron(III), Talanta 21 (1974) 314–318, https://doi.org/10.1016/0039-9140(74)80012-3.
[23] I. Noda, Techniques of two-dimensional (2D) correlation spectroscopy useful in life, Biomed. Spectrosc. Imaging 4 (2015) 109–127, https://doi.org/10.3233/BSI-150105.
[24] P. Weppen, A. Hornburg, Calorimetric studies on interactions of divalent cations and microorganisms or microbial envelopes, Thermochim. Acta 269–270 (1995) 393–404, https://doi.org/10.1016/0040-6031(95)02515-4.
[25] R.L. Blake, R.E. HessevicK, T. Zoltai, L.W. Finger, Refinement of the hematite structure, Am. Mineral. 51 (1966) 123–129, https://doi.org/10.1016.2010.01.025.
[26] G.A. Waychunas, Structure, aggregation and characterization of nanoparticles, Rev. Mineral. Geochem. 44 (2001) 104–166, https://doi.org/10.2138/rmg.2001.44.04.
[27] K. Kandori, G. Yonekawa, Preparation and characterization of uniform pseudocubic hematite particles by utilizing polyethylene oxide polymers in forced hydrolysis reaction, J. Ceram. Soc. Jpn. 122 (2014) 795–801, https://doi.org/10.2109/jcersj2.122.795.
[28] S. Sahoo, K. Agarwal, A. Singh, B. Polke, K. Raha, Characterization of γ- and α-Fe_2O_3 and α-Fe_2O3 nano powders synthesized by emulsion precipitation-calcination route and rheological behaviour of α-Fe_2O_3, Int. J. Eng. Sci. Technol. 2 (2011), https://doi.org/10.4314/ijest.v2i8.63841.
[29] A. Lassoued, B. Dkhil, A. Gadri, S. Ammar, Control of the shape and size of iron oxide (α-Fe_2O_3) nanoparticles synthesized through the chemical precipitation method, Results Phys. 7 (2017) 3007–3015, https://doi.org/10.1016/j.rinp.2017.07.066.
[30] A.S. Madden, M.F. Hochella, T.P. Luxton, Insights for size-dependent reactivity of hematite nanomineral surfaces through Cu^{2+} sorption, Geochim. Et. Cosmochim. Acta 70 (2006) 4095–4104, https://doi.org/10.1016/j.gca.2006.06.1366.
[31] W. Zhao, S.L. Walker, Q. Huang, P. Cai, Contrasting effects of extracellular polymeric substances on the surface characteristics of bacterial pathogens and cell attachment to soil particles, Chem. Geol. 410 (2015) 79–88, https://doi.org/10.1016/j.chemgeo.2015.06.013.
[32] J. Bosch, K. Heister, T. Hofmann, R.U. Meckenstock, Nanosized iron oxide colloids strongly enhance microbial iron reduction, Appl. Environ. Microbiol. 76 (2010) 184–189, https://doi.org/10.1128/AEM.00417-09.
[33] K. Werellapatha, K.M. Kuhn, B.A. Bunker, P.A. Maurice, Nanoparticle size effects on cadmium uptake on hematite: revisiting the sorption edge approach, Environ. Eng. Sci. 36 (2019) 883–891, https://doi.org/10.1089/ees.2019.0105.
[34] S. Gogoi, S. Chakraborty, M.D. Saikia, Surface modified pineapple crown leaf for adsorption of Cr(VI) and Cr(III) ions from aqueous solution, Biochem. Pharmacol. (2018), https://doi.org/10.1016/j.jece.2018.03.040.
[35] A. Mohamed, L. Yu, Y. Fang, N. Ashry, Y. Riahi, I. Uddin, Q. Huang, Iron mineral-humic acid complex enhanced Cr(VI) reduction by *Shewanella oneidensis* MR-1, Chemosphere 247 (2020), 125902, https://doi.org/10.1016/j.chemosphere.2020.125902.
[36] B.F. Lavallée, F.R. Pick, Picocyanobacteria abundance in relation to growth and loss rates in oligotrophic to mesotrophic lakes, Aquat. Microb. Ecol. 27 (2002) 37–46, https://doi.org/10.3354/ame027037.
[37] W. Yan, H. Wang, C. Jing, Adhesion of *Shewanella oneidensis* MR-1 to goethite: a two-dimensional correlation spectroscopic study, Environ. Sci. Technol. 50 (2016) 4343–4349, https://doi.org/10.1021/acs.est.6b00066.
[38] A.S. Gordon, F.J. Millero, S.M. Gerchakov, Microcalorimetric measurements of glucose metabolism by marine bacterium *Vibrio alginolyticus*, Appl. Environ. Microbiol. 44 (1982) 1102–1109, https://doi.org/10.1128/aem.44.5.1102-1109.1982.
[39] S. Ma, C.S. Song, Y. Chen, F. Wang, H.L. Chen, Hematite enhances the removal of Cr(VI) by *Bacillus subtilis* BSn5 from aquatic environment, Chemosphere 208 (2018) 579–585, https://doi.org/10.1016/j.chemosphere.2018.06.037.
[40] G. Stotzky, Influence of Soil Mineral Colloids on Metabolic Processes, Growth, Adhesion, and Ecology of Microbes and Viruses, U.S. Environmental Protection Agency, Washington, D.C., 1986, pp. 305–428, https://doi.org/10.2136/sssaspecpub17.c10. EPA/600/D-88/161 (NTIS PB88237946).
[41] T. Liu, X. Luo, Y. Wu, J.R. Reinfelder, X. Yuan, X. Li, D. Chen, F. Li, Extracellular electron shuttling mediated by soluble c-type cytochromes produced by *Shewanella oneidensis* MR-1, Environ. Sci. Technol. 54 (2020) 10577–10587, https://doi.org/10.1021/acs.est.9b06868.
[42] C. Kang, P. Wu, Y. Li, B. Ruan, L. Li, L. Tran, N. Zhu, Z. Dang, Understanding the role of clay minerals in the chromium(VI) bioremoval by *Pseudomonas aeruginosa* CCTCC AB93066 under growth condition: microscopic, spectroscopic and kinetic analysis, World J. Microbiol. Biotechnol. 31 (2015) 1765–1779, https://doi.org/10.1007/s11274-015-1928-9.
[43] C. Qu, S. Qian, L. Chen, Y. Guan, L. Zheng, S. Liu, W. Chen, P. Cai, Q. Huang, Size-dependent bacterial toxicity of hematite particles, Environ. Sci. Technol. 53 (2019) 8147–8156, https://doi.org/10.1021/acs.est.9b00856.
[44] X.Q. Li, J. Cao, W.X. Zhang, Stoichiometry of Cr(VI) immobilization using nanoscale zero valent iron (nZVI): a study with high-resolution X-ray photoelectron spectroscopy (HR-XPS), Ind. Eng. Chem. Res. 47 (2008) 2131–2139, https://doi.org/10.1021/ie061655x.
[45] S.H. Zhang, M.F. Wu, T.T. Tang, Q.J. Xing, C.Q. Peng, F. Li, H. Liu, X.B. Luo, J. P. Zou, X.B. Min, J.M. Luo, Mechanism investigation of anoxic Cr(VI) removal by nano zero-valent iron based on XPS analysis in time scale, Chem. Eng. J. 335 (2018) 945–953, https://doi.org/10.1016/j.cej.2017.10.182.
[46] P. Wu, S. Li, L. Ju, N. Zhu, J. Wu, P. Li, Z. Dang, Mechanism of the reduction of hexavalent chromium by organo-montmorillonite supported iron nanoparticles, J. Hazard. Mater. 219–220 (2012) 283–288, https://doi.org/10.1016/j.jhazmat.2012.04.008.
[47] H. Jiang, X. Han, Z. Li, X. Chen, Y. Hou, L. Gai, D. Li, X. Lu, T. Fu, Superparamagnetic core-shell structured microspheres carrying carboxyl groups as adsorbents for purification of genomic DNA, Colloids Surf. A Physicochem. Eng. Asp. 401 (2012) 74–80, https://doi.org/10.1016/j.colsurfa.2012.03.024.
[48] C. Zhu, F. Liu, Y. Zhang, M. Wei, X. Zhang, C. Ling, A. Li, Nitrogen-doped chitosan-Fe(III) composite as a dual-functional material for synergistically enhanced co-removal of Cu(II) and Cr(VI) based on adsorption and redox, Chem. Eng. J. 306 (2016) 579–587, https://doi.org/10.1016/j.cej.2016.07.096.
[49] S. Sitthichai, C. Pilapong, T. Thongtem, S. Thongtem, CMC-coated Fe_3O_4 nanoparticles as new MRI probes for hepatocellular carcinoma, Appl. Surf. Sci. 356 (2015) 972–977, https://doi.org/10.1016/j.apsusc.2015.08.140.
[50] J. Lu, F. Fu, L. Zhang, B. Tang, Insight into efficient co-removal of Se(IV) and Cr(VI) by magnetic mesoporous carbon microspheres: performance and mechanism, Chem. Eng. J. 346 (2018) 590–599, https://doi.org/10.1016/j.cej.2018.04.077.
[51] C. Xu, W. Yang, W. Liu, H. Sun, C. Jiao, A. jun Lin, Performance and mechanism of Cr(VI) removal by zero-valent iron loaded onto expanded graphite, J. Environ. Sci. 67 (2018) 14–22, https://doi.org/10.1016/j.jes.2017.11.003.
[52] D. Chang, T. Chen, H. Liu, Y. Xi, C. Qing, Q. Xie, R.L. Frost, A new approach to prepare ZVI and its application in removal of Cr(VI) from aqueous solution, Chem. Eng. J. 244 (2014) 264–272, https://doi.org/10.1016/j.cej.2014.01.095.